Synthesis of Crystalline Microporous Mo−V−Bi Oxide for Selective (Amm)Oxidation of Light Alkanes

Satoshi Ishikawa,[†] Yoshinori Goto,[‡] Yoshito Kawahara,[†] Shoma Inukai,[†] Norihito Hiyoshi,[§] Nicholas F. Dummer,[∥] Toru Murayama,[⊥] Akihiro Yoshida,[†] Masahiro Sadakane,[#] and Wataru Ueda*[,†]

[†]Department of Material and Life Chemistry, Faculty of Engineering, Kanagawa University, 3-27-1 Rokkakubashi, Kanagawa-ku, Yokohama 221-8686, Japan

[‡]Catalysis Research Center, Hokkaido University, N-21, W-10, Sapporo 001-0021, Japan

[§]National Institute of Advanced Industrial Science and Technology (AIST), 4-2-1 Nigatake, Miyagino, Sendai 983-8551, Japan

[∥]Cardiff Catalysis Institute, School of Chemistry, Cardiff University, Main Building, Park Place, Cardiff, CF10 3AT, United Kingdom

[⊥]Department of Applied Chemistry, Graduate School of Urban Environmental Sciences, Tokyo Metropolitan University, 1-1 minami-osawa, Hachioji, Tokyo 192-0397, Japan

[#]Department of Applied Chemistry, Graduate School of Engineering, Hiroshima University, 1-4-1 Kagamiyama, Higashi-Hiroshima 739-8527, Japan

* Supporting Information

ABSTRACT: Bismuth (Bi) was successfully introduced into the crystalline orthorhombic Mo_3VO_x (MoVO) structure for the first time by using the ethylammonium cation ($EtNH_3^+$) as a structure-directing agent in hydrothermal synthesis, and the catalytic activities of MoVO-containing Bi (MoVBiO) for selective oxidation of ethane and ammoxidation of propane were compared with those of ternary MoVO. Bi and $EtNH_3^+$ were located in hexagonal and heptagonal channels in the MoVO structure, respectively. $EtNH_3^+$ could be removed without collapse of the crystal structure by appropriate heat treatment, leaving the heptagonal channels empty. The introduction of Bi had only a little effect on the catalytic activity for selective oxidation of ethane. On the other hand, the conversion of propane was significantly enhanced in propane ammoxidation. Acrylonitrile selectivity was also enhanced by the introduction of Bi, especially at high temperatures (>440 °C).

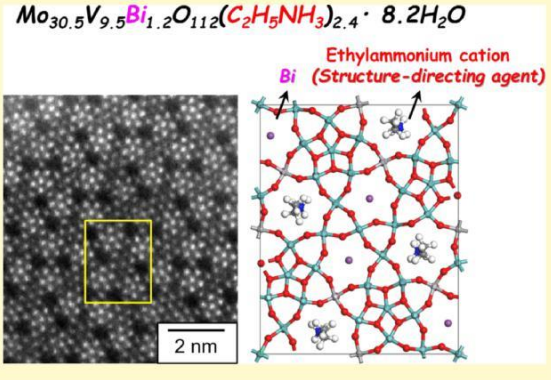

INTRODUCTION

Multifunctionalization of catalysts is an attractive research topic for improving their catalytic activity.[1−5] Generally, this concept is important in selective oxidation as the reaction is comprised of many elementary steps, including C−H activation, adsorption of reaction intermediates, oxygen insertion, and desorption of products. Therefore, many catalytic functions should be accumulated in order to achieve high product selectivities.[6,7] For multifunctionalization of a catalyst, nano-level structural control and a suitable elemental arrangement are essential. For the structural aspect, effective catalysts require the sites to trap and polarize substrates such as micropores.[4,5] For the elemental arrangement, suitable elements having different catalytic roles should cooperate not only for facilitating the conversion of substrates and intermediates but also for facile desorption of oxidation products.[8−10] Accord-ingly, the construction of a highly organized crystal structure with an appropriate elemental arrangement is one way to realize the evolution of oxidation catalysts.[1,8−11]

Crystalline Mo_3VO_x oxide (MoVO) has attracted much attention as an effective catalyst for selective oxidation of alkanes, alcohols, and aldehydes.[12−20] The catalytic activity of MoVO is largely derived from its sophisticated crystal structure.[13− 15,18−20] Figure 1 shows the crystal structure of MoVO. The arrangement of pentagonal $\{Mo_6O_{21}\}^{6-}$ units and pentamer units comprised of five MO_6 (M = Mo, V) octahedral units forms a highly organized crystal structure with two types of micropores, hexagonal, and heptagonal channels.[15] In the selective oxidation of ethane and acrolein, we have reported that the heptagonal channel effectively traps substrates and that the pentamer unit adjacent to the heptagonal channel works as an active center, realizing an extremely high catalytic activity.[21−23] The unique feature of MoVO is that this material is amenable to the introduction of other elements into and substitution of elements in the crystal structure without

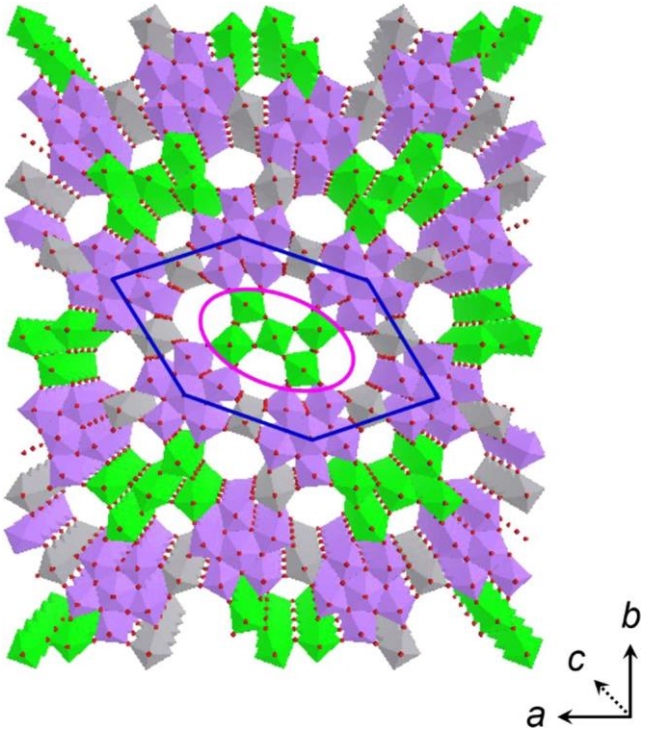

Figure 1. Structural model of crystalline orthorhombic Mo−V oxide. Blue enclosure represents the network structure based on the arrangement of the pentagonal $\{Mo_6O_{21}\}^{6-}$ unit and VO_6 octahedral. The pink circle represents the pentamer unit embedded into the void of the network structure. Mo, purple; V, gray; and mixture of Mo and V, green.

changing the basic crystal structure.[24−28] For selective (amm)-oxidation of propane to form acrylic acid or acrylonitrile, the introduction of other elements into and substitution of elements in the MoVO structure strongly affect its catalytic performance. For example, the introduction of Te or Sb into the hexagonal channel drastically enhances the selectivity to acrylic acid or acrylonitrile, and the partial substitution of Mo in the pentagonal $\{Mo_6O_{21}\}^{6-}$ unit with Nb further increases the selectivity.[29−36] The effects of the introduction of Te or Sb into the hexagonal channel are crucial. The insertion of Te or Sb results in smooth abstraction of the α-hydrogen from propylene (primary product of propane (amm)oxidation), which facilitates the sequential (amm)oxidation of propylene to form acrylic acid or acrylonitrile.[37−41]

For selective (amm)oxidation of propylene, Mo-Bi-based mixed metal oxides are well-known as extremely active catalysts and have been industrialized.[10,33,42−45] In these catalysts, it has been reported that Bi abstracts the α-hydrogen from propylene at the first step of the reaction, the same as the role of Te and Sb in MoV(Te or Sb)O catalysts.[33,46−48] Therefore, the introduction of Bi into MoVO is thought to enhance the selectivity to acrylic acid or acrylonitrile in the selective (amm)oxidation of propane in the same manner as Te and Sb. In addition, Bi is thermally stable, and sublimation is thus not likely to occur as with Te. Moreover, the strong basic character of Bi is expected to suppress an acidic character of the catalyst, which can lead easy desorption of oxygenated products from the catalyst surface, resulting in a decrease in overoxidation rates. On the basis of this perspective, the introduction of Bi into MoVO has been strongly desired for a long time. However, introduction of Bi into the MoVO structure has not been reported to date, despite considerable efforts.[49−51]

In this paper, we describe the successful synthesis of a crystalline orthorhombic Mo−V−Bi oxide (MoVBiO) for the first time without altering the framework structure of MoVO. In addition to the method for synthesis of MoVBiO, detailed characteristics and catalytic performance of MoVBiO for selective (amm)oxidation of ethane and propane are shown. We believe that the findings discussed here will contribute to a catalyst design rationale and to the development of the next highly effective catalysts for selective oxidations.

EXPERIMENTAL SECTION

Synthesis of an Orthorhombic Mo_3VO_x Catalyst. Orthorhom-bic Mo_3VO_x (MoVO) was synthesized by a hydrothermal method. First, 8.828 g of $(NH_4)_6Mo_7O_{24}\cdot 4H_2O$ (Mo: 50 mmol, Wako) was dissolved in 120 mL of distilled water. Separately, an aqueous solution of $VOSO_4$ was prepared by dissolving 3.288 g of hydrated $VOSO_4$ (V: 12.5 mmol, Mitsuwa Chemicals) in 120 mL of distilled water. The two solutions were mixed at ambient temperature and stirred for 10 min. The mixed solution (pH 3.2) was placed in an autoclave that had a 300 mL Teflon inner vessel with a thin Teflon sheet of 4000 cm^2 in size covering about half of the Teflon inner vessel space. Then N_2 was fed into the solution through a tube to remove residual oxygen. This step is necessary to obtain well-crystallized material since residual oxygen in the solution oxidizes the intermediate for forming MoVO, resulting in poor crystalline material. Then the hydrothermal reaction was carried out at 175 °C for 48 h under static conditions in an electric oven. The gray solids that formed were washed with distilled water and dried in air at 80 °C overnight. The material obtained is denoted as MoVO-fresh. Then purification with oxalic acid was conducted in order to remove the impurity. To 25 mL of an aqueous solution (0.4 mol L^{-1}, 60 °C) of oxalic acid (Wako), 1 g of MoVO-fresh was added and stirred for 30 min, and then the solid material collected by filtration was washed with 500 mL of distilled water. The sample after purification is abbreviated as MoVO. If needed, MoVO was calcined under static air or 50 mL min^{-1} of nitrogen flow for 2 h at 400 °C. The recovered material is abbreviated as MoVO-AC (air calcination) or MoVO-NT (heat treatment under nitrogen flow).

Synthesis of an Mo−V−Bi Oxide Catalyst. For synthesizing Mo−V−Bi oxide (MoVBiO), ethylammonium trimolybdate [EATM, $(CH_3CH_2NH_3)_2Mo_3O_{10}$] was used as an Mo source instead of $(NH_4)_6Mo_7O_{24}\cdot 4H_2O$ (AHM). EATM was prepared as described previously.[52,53] First, 21.594 g of MoO_3 (0.150 mol, Kanto) was dissolved in 28.0 mL of 70% ethylamine solution (ethylamine: 0.300 mol, Wako) diluted with 28.0 mL of distilled water. The reason for the addition of distilled water was to reduce the viscosity of the mixed solution. After being completely dissolved, the solution was evaporated under vacuum (P/P_0 = 0.03) at 70 °C, and then a solid powder was obtained. The powder was dried in air at 80 °C overnight.

Then, 1.799 g of EATM (Mo: 10 mmol) was dissolved in 20 mL of distilled water. Separately, an aqueous solution of $VOSO_4$ was prepared by dissolving 0.658 g of hydrated $VOSO_4$ (V: 2.5 mmol) in 20 mL of distilled water. The two solutions were mixed and stirred for 10 min at ambient temperature before the addition of 0.326 g of BiOCl (Bi: 1.25 mmol, Wako). The pH value of the solution was not changed by the addition of the Bi source and was 2.4. The pH value of the solution was then reduced to 2.0 by the addition of 2 M H_2SO_4 (ca. 200 μL). The mixed solution was placed in an autoclave that had a 50 mL Teflon inner vessel with a thin Teflon sheet of 800 cm^2 in size covering about half of the Teflon inner vessel space. Then N_2 was fed into the solution to remove residual oxygen. The hydrothermal reaction was then carried out at 175 °C for 48 h with rotation at 1 rpm. Rotation was needed for the dissolution of the Bi source since the Bi source was hardly dissolved under static conditions. The solid obtained by the hydrothermal synthesis was separated by filtration, washed with distilled water, and dried in air at 80 °C overnight. The material obtained is abbreviated as MoVBiO-fresh. In order to remove

the impurity related to Bi, purification with hydrochloric acid was carried out for MoVBiO-fresh. To 25 mL of an aqueous solution (1.2 M, 25 °C) of hydrochloric acid (Wako), 1 g of dried MoVBiO-fresh was added and stirred for 30 min and then washed with 1000 mL of distilled water after filtration. The material obtained is abbreviated as MoVBiO. After washing with distilled water, almost no Cl remained on the MoVBiO surface as confirmed by XPS (Figure S1). If needed, MoVBiO was calcined under static air or 50 mL min^{-1} of N_2 flow at 400 °C for 2 h. The material obtained after heat treatment is abbreviated as MoVBiO-AC (air calcination) or MoVBiO-NT (heat treatment under N_2). The material obtained when no Bi source was added in this synthesis is denoted as MoVO (EATM)-fresh. MoVO (EATM)-fresh was purified with oxalic acid in the same manner as that for MoVO-fresh. Purified MoVO (EATM)-fresh is denoted as MoVO (EATM). For a comparison, Mo−V−Bi oxide was synthesized using $(NH_4)_6Mo_7O_{24}{\cdot}4H_2O$ (AHM) as a Mo precursor. First, 1.766 g of AHM (Mo: 10 mmol) was dissolved in 20 mL of distilled water. This solution was mixed with an aqueous solution prepared by dissolving 0.658 g of hydrated $VOSO_4$ (V: 2.5 mmol) in 20 mL of distilled water. The two solutions were mixed at ambient temperature and stirred for 10 min before the addition of 0.326 g of BiOCl (Bi: 1.25 mmol). Then the pH value of the solution was reduced to 2.0 by the addition of 2 M H_2SO_4 (no pH control: pH = 3.1). After the reduction of pH, N_2 bubbling was carried out for 10 min. Then the hydrothermal reaction was carried out at 175 °C for 48 h with rotation at 1 rpm. The material that had formed was separated by filtration, washed with distilled water, and dried in air at 80 °C overnight. The material obtained is abbreviated as MoVBiO (AHM)-fresh.

Characterization of Materials. The materials obtained were characterized by the following techniques. Powder XRD patterns were recorded with a diffractometer (RINT Ultima+, Rigaku) using Cu Kα radiation (tube voltage: 40 kV, tube current: 40 mA). For XRD measurements, the samples were ground with Si standard (NIST) for 5 min in order to correct the peak position and to exclude an orientation effect. Diffractions were recorded in the range of 4°~80° with a scan speed of 1° min^{-1}. FT-IR analysis was carried out using a spectrometer (FT/IR-660, JASCO) with an MCT detector. IR spectra were obtained by integration of 256 scans with a resolution of 4 cm^{-1}. CHN elemental analysis was conducted using Micro Corder JM10 (Yanaco). XPS (JPC-9010MC, JEOL) with nonmonochromatic Mg Kα radiation was used for measuring binding energy values of Mo, V, Bi, and Cl. Temperature-programmed desorption of ammonia (NH_3-TPD) was used to measure oxide surface acidity. The experiment was carried out using an auto chemisorption system (BEL JAPAN). The experimental procedure was as follows. The sample (ca. 50 mg) was sandwiched by two layers of quartz wool and preheated under He (50 mL min^{-1}) for 10 min at 400 °C. Then 50 mL min^{-1} of 12.5% NH_3/He was introduced at 200 °C for 30 min, followed by flushing with He for 30 min at the same temperature. The desorption profile from 200 to 600 °C was recorded with a mass spectrometer under He flow (50 mL min^{-1}). Temperature-programmed desorption (TPD) was carried out with the same apparatus and same sample amount. The temperature was increased from 40 to 600 °C. STEM-EDX analysis was carried out with HD-2000 (Hitachi). For STEM analysis, samples were dispersed in ethanol and treated by ultrasonic equipment. The supernatant liquid was dropped on the Cu-grid and dried overnight for the measurement. SEM analysis was carried out with an electron microscope (JSM-7400F, JEOL). Elemental compositions in the bulk were determined by ICP-AES (ICPE-9000, Shimadzu). N_2 adsorption isotherms at liq. N_2 temperature were obtained using an autoadsorption system (BELSORP MAX, Nippon BELL). External surface area and micropore volume were determined by the t-plot method. Prior to the N_2 adsorption, the samples were heat-treated under a vacuumed condition for 2 h at 300 °C. The uncalcined sample was pretreated under the same condition but at 100 °C. Propane adsorption was carried out with the same apparatus at 25 °C. Prior to the propane adsorption, the samples were heat-treated under a vacuumed condition at 300 °C for 2 h. Micropore volume was estimated by the DA method when propane adsorption was conducted. Aberration-corrected STEM images of MoVBiO were obtained using ARM-200F (JEOL Ltd., Japan) equipped with a cold field emission gun at an acceleration voltage of 200 kV. The convergence semiangle of the probe was 24 mrad. The collection semiangle for high angle annular dark field (HAADF) imaging was adjusted in the range of 68−175 mrad. Images were treated with a light low-pass filter using a 3 × 3 kernel (Digital Micrograph, Gatan Inc.) to remove high-frequency noise. The powder diffraction program of Materials Studio 7.1 (Accelrys) was used for an XRD simulation experiment. XRD simulation was carried out by changing the Bi occupancy in the basic crystal structure of MoVO obtained by single crystal analysis.[54] In this experiment, Bi was set into the hexagonal channel of the basic crystal structure and the Bi occupancy was changed from 0% to 30%. The Rietveld program of Materials Studio 7.1 (Accelrys) was used for Rietveld refinement. The XRD patterns after correcting the peak position with Si were subjected to the refinement. The occupancy of metals in the framework (comprised of Mo and V) and temperature factors of all atoms were fixed without further refinement from the structural model of MoVO obtained by single crystal analysis.[54] As shown in Results and Discussion, Bi is located at the hexagonal channel, and $EtNH_3^+$ is located at the heptagonal channel with a vertical configuration. Occupancy of Bi and $EtNH_3^+$ were determined by ICP and CHN elemental analyses. All metal positions were refined. After the refinement of metal positions, oxygen atom positions were refined to set a proper metal−oxygen length. The position of $EtNH_3^+$ was difficult to refine due to its low molecular weight, and the position of $EtNH_3^+$ in the structure was therefore fixed at the position where the distance of lattice oxygen to $EtNH_3^+$ is proper. The pattern parameters were refined for obtaining the lowest R_{wp} value. Atom positions are shown in Table S1, and Rietveld analysis parameters are shown in Table S2.

Catalytic Test. Selective oxidation of ethane in the gas phase was carried out at atmospheric pressure in a conventional vertical flow system with a fixed bed Pyrex tubular reactor. First, 0.50 g of the catalyst was diluted with 2.10 g of silica and put into the tubular reactor for ethane oxidation. The reactor was heated gradually from room temperature at a rate of 10 °C min^{-1} to 350 °C under nitrogen flow (40 mL min^{-1} from the top of the reactor). The temperature was measured with a thermocouple inserted in the middle of the catalyst zone. When the temperature reached 350 °C, a reactant gas with the composition of $C_2H_6/O_2/N_2$ = 10/10/80 (mol %) was fed in at a total flow rate of 50 mL min^{-1}. After holding for 2 h in this condition, the reaction was started. After analysis at this reaction temperature, the reaction temperature was decreased to 330, 310, 290, 270, and 250 °C. Reactants and products were analyzed with three online gas chromatographs (Molecular Sieve 13× for O_2, N_2, and CO with a TCD detector, Gaskuropack54 for CO_2, C_2H_4, and C_2H_6 with a TCD detector, and Porapak Q for acetic acid with an FID detector). A blank run showed that homogeneous gas-phase reactions were negligible under the experimental conditions used in this study. Carbon balance was always ca. 98−100%, and the product selectivity was thus calculated on the basis of the product sum.

Ammoxidation of propane was carried out at atmospheric pressure in the same conventional vertical flow system with a Pyrex tubular reactor. First, 0.10−0.30 g of the catalyst was diluted with 5.00 g of SiC and put into the tubular reactor. The reactor was heated at a rate of 10 °C min^{-1} under 50 mL min^{-1} of N_2 flow. When the temperature reached 420 °C, 50 mL min^{-1} of reactant gas with the composition of $C_3H_8/O_2/NH_3/He$ = 6.0/18.0/8.0/68.0 (mol %) was fed in and held for 30 min at the same temperature. Propane ammoxidation was carried out at each reaction temperature with decreases in the reaction temperature to 410, 400, 390, and 380 °C. As an external standard for GC analysis, 10 mL min^{-1} of CH_4 was mixed from the outlet of the reactor. Reactants and products were analyzed with three online gas chromatographs (Molecular Sieve 13× for O_2, N_2, CH_4, and CO with a TCD detector, Gaskuropack54 for CO_2, NH_3, C_3H_6, and C_3H_8 with a TCD detector, and Porapak QS for C_2H_3N and C_3H_3N with an FID detector). A blank run showed that no reaction took place without catalysts under the experimental conditions used in this study. Carbon balance was always ca. 95−105%.

RESULTS AND DISCUSSION

Synthesis of Crystalline Mo−V−Bi Oxide. Figure 2 shows XRD patterns of MoVO, MoVO (EATM), and MoVBiO. MoVO showed XRD peaks at 6.7°, 7.9°, 9.0°, and 22.2°, which were attributed to the diffraction of (020), (120), (210), and (001) planes of MoVO, respectively [Figure 2A (a)].[15,54] No XRD peaks related to impurities were observed, indicating a high purity of this material. When $(C_2H_5NH_3)_2Mo_3O_{10}$ (EATM) was used as the Mo source instead of $(NH_4)_6Mo_7O_{24}\cdot 4H_2O$ (AHM), the formation of an amorphous type of Mo_3VO_x that is crystallized only in the rod direction (c direction) and not in the cross section (a-b plane) was observed as we reported previously [Figure 2A (b)].[15,52] On the other hand, surprisingly, a material showing the same XRD pattern as that of MoVO was formed when the Bi source was used together with EATM [Figure 2A (c)]. The use of AHM as the Mo source in the presence of the Bi source led to the formation of MoO_3 and ε-Keggin polyoxometalate-based porous material ($(NH_4)_{2.8}H_{0.9}[\varepsilon\text{-}VMo_{9.4}V_{2.6}O_{40}Bi_2]$) (Figure S2).[55−57] This fact suggests that ethylammonium cation ($EtNH_3^+$) is essential for formation of the MoVO structure when the Bi source is added. Figure 2B shows XRD patterns of MoVO, MoVO (EATM), and MoVBiO measured from 21.5° to 23.0°. MoVO and MoVO (EATM) showed diffraction peaks of (001) at the same position (at 22.22°) despite different counter cations being used in the preparation. On the other hand, a downward shift of this peak was observed in MoVBiO (22.18°) compared with those of the two samples. Lattice parameters of MoVO and MoVBiO are shown in Table 1. The lattice parameters of MoVO were a = 2.106 nm, b = 2.650 nm, and c = 0.3999 nm, which matched well with our previous report.[15,52,54] The lattice parameters of MoVBiO, a = 2.117 nm, b = 2.657 nm, and c = 0.4007 nm, were much larger than those of MoVO. Since the type of countercation caused no apparent changes in lattice parameters as can be seen by a comparison of MoVO and MoVO (EATM), the observed lattice expansion would have been caused by the introduction of Bi inside the MoVO structure. Comparable expansion has been observed when Te or Sb was introduced into the hexagonal channel of the MoVO structure.[31,58]

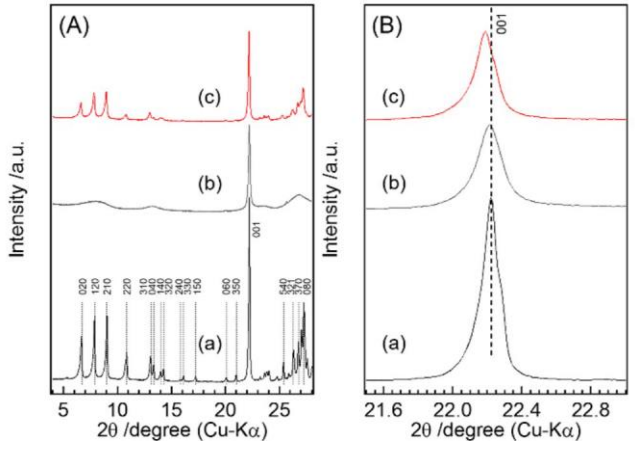

Figure 2. (A) XRD patterns of (a) MoVO, (b) MoVO (EATM), and (c) MoVBiO. (B) Enlarged XRD patterns of (a) MoVO, (b) MoVO (EATM), and (c) MoVBiO measured from 21.5° to 23.0°. The black bar in (B) represents the peak position of 22.2° of MoVO that is derived from stacking of the a−b plane in the c direction [(001) plane].

The morphology, elemental distribution, and elemental composition of MoVBiO were evaluated by SEM, STEM-EDX, and STEM-mapping analyses. Figure 3 shows SEM and

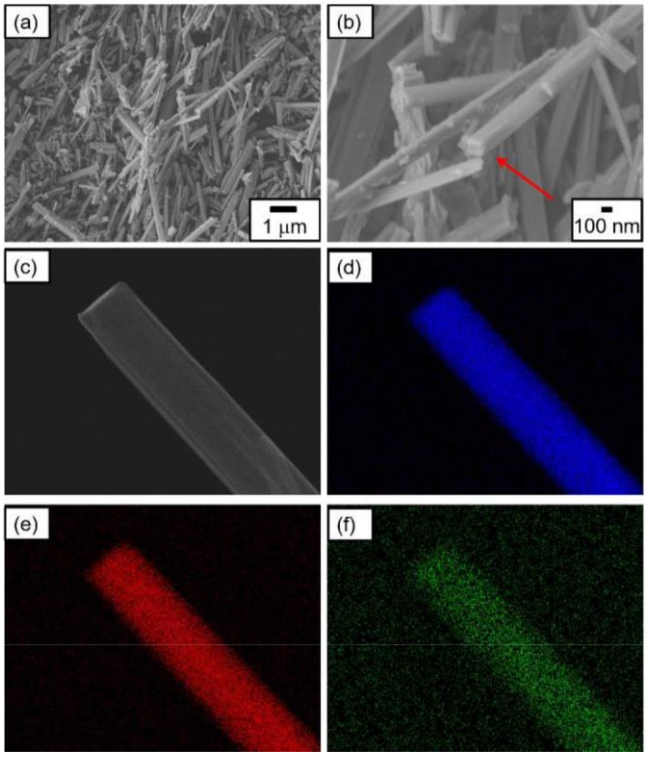

Figure 3. (a and b) SEM images and (c−f) STEM-mapping images of MoVBiO. (c) STEM image, (d) mapping image of Mo, (e) mapping image of V, and (f) mapping image of Bi. The red arrow in (b) shows the crystal habit of MoVBiO.

Table 1. Physicochemical Properties of MoVO and MoVBiO

	lattice parameters[a] (nm)			elemental composition ratio (Mo/V/Bi)				
catalyst	a	b	c	rod-shaped crystal (EDX)	bulk (ICP)	elemental composition of catalyst[b]	external surface area[c] ($m^2\ g^{-1}$)	micropore volume[c] (10^{-3} $cm^3\ g^{-1}$)
MoVO	2.105(6)	2.649(8)	0.3999(1)	–	1/0.38/0	$Mo_{28.6}V_{11.4}O_{112}(NH_4)_{3.7}\cdot 10.0H_2O$	5.8	13.0
MoVBiO	2.116(8)	2.656(7)	0.4006(6)	1/0.31/0.06	1/0.31/0.04	$Mo_{30.5}V_{9.5}Bi_{1.2}O_{112}(C_2H_5NH_3)_{2.3}\cdot 8.2H_2O$	9.5	11.6

[a]Determined by Rietveld refinement. [b]Determined by the results of ICP and CHN elemental analysis. [c]Measured by N_2 adsorption at liq. N_2 temperature and estimated by the t-plot method.

STEM-mapping images of MoVBiO. MoVBiO was a rod-shaped crystal in a reflection of stacking of the a–b plane along the c-direction. The cross section of the rod (a–b plane) was a rectangle shape (shown by a red arrow in Figure 3b), indicating the crystal habit of this material. The diameter of the rods was ca. 0.19 μm in the average of 50 crystallites, being almost half the size of MoVO (0.42 μm). We have reported that the diameters of rods of MoVO decreased when alkylammonium isopolymolybdates were used as Mo sources.[52] Thus, the observed decrease in rod diameter might be derived from the effect of $EtNH_3^+$ on the crystal formation process. STEM-mapping images of the rod are shown in Figure 3 (panels c~f). It was found that Mo, V, and Bi were uniformly distributed throughout the rod. Elemental composition of the rod was estimated at the same time by STEM-EDX and is shown in Table 1. The elemental composition of MoVBiO was Mo/V/Bi = 1/0.31/0.06, which is consistent with the elemental composition estimated by ICP (Mo/V/Bi = 1/0.31/0.04). Since the elemental compositions of the bulk (estimated by ICP) and the rod-shaped crystal (estimated by STEM-EDX) were almost the same, it is thought that MoVBiO is highly pure and that almost no impurities are present in the material. This fact is in line with the results of XRD. The V/Mo ratio of MoVO was 0.38, which was slightly higher than that of MoVBiO. For this decreased V content, we have reported that the V/Mo ratio decreased when alkylammonium isopolymo-lybdates were used as Mo sources.[52]

Figure 4 shows the IR spectra of MoVO and MoVBiO. Both of the materials showed IR bands at 915 cm^{-1} that were

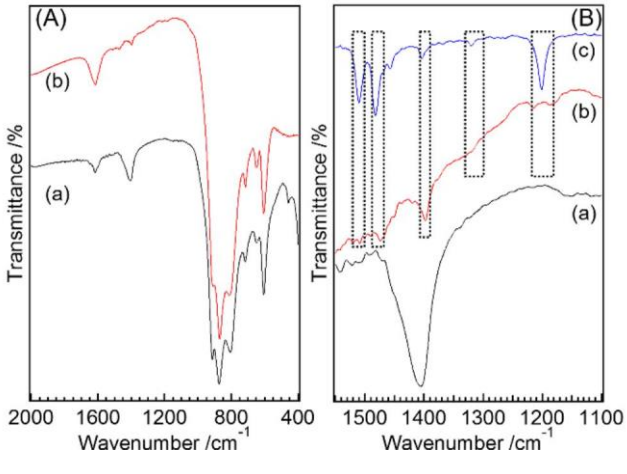

Figure 4. (A) IR spectra of (a) MoVO and (b) MoVBiO. (B) Enlarged IR spectra of (a) MoVO, (b) MoVBiO, and (c) EATM from 1100 to 1550 cm^{-1}. The dotted line in (B) represents the absorption derived from $EtNH_3^+$.

attributable to V = O, 874, 840, 817, 800, 720, and 652 cm^{-1} for Mo–O–Mo, 604 cm^{-1} for V–O–Mo, and 458 cm^{-1} for Mo–O.[15,54] All of these bands were characteristic for MoVO. Since no differences in IR bands derived from the framework structure consisting of Mo and V were observed between MoVO and MoVBiO, Bi might be placed at a site away from the framework structure. Figure 4B shows enlarged IR spectra from 1100–1550 cm^{-1}. MoVO showed an IR band at 1401 cm^{-1} that was attributed to an asymmetric deformation vibration of NH_4^+. It has been reported that NH_4^+, a countercation of the Mo source, is occluded in the heptagonal channel during the crystal formation process.[52] MoVBiO showed IR bands at 1188 and 1215 cm^{-1} attributed to CH_3 rocking, at 1317 cm^{-1} attributed to CH_2 twisting, at 1397 cm^{-1} attributed to CH_3 scissoring, at 1474 cm^{-1} attributed to CH_2 scissoring, and at 1508 cm^{-1} attributed to NH_3^+ scissoring. These bands were also observed in EATM, indicating the presence of $EtNH_3^+$ in MoVBiO.[59–61] This fact can also be confirmed by TPD analysis as shown later. Since MoVBiO was formed only when $EtNH_3^+$ was used, $EtNH_3^+$ might act as a structure-directing agent for formation of the MoVO structure. In the next section, the location sites of Bi and $EtNH_3^+$ in the MoVO structure are discussed.

Location Sites of Bi and $EtNH_3^+$ in MoVBiO. First, the location site of Bi was investigated. As stated in the previous section, IR absorption implied that Bi is located at a site away from the framework structure consisting of Mo and V. In order to reveal the location site of Bi, HAADF-STEM analysis was carried out. HAADF-STEM is a useful method for analyzing the positions of heavy metals because the intensity of the white spot is roughly proportional to the square of the atomic number (Z), providing an enhanced Z-constant image.[62,63] Figure 5 shows an HAADF-STEM image of MoVBiO in the

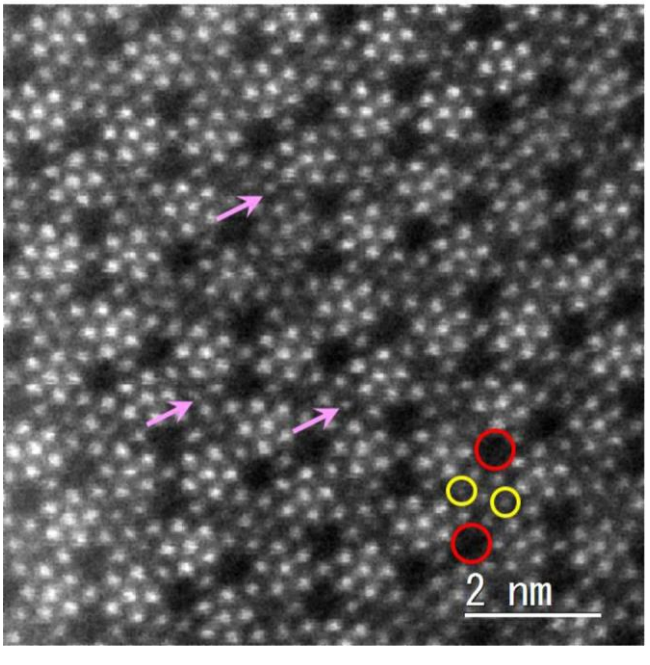

Figure 5. HAADF-STEM image of MoVBiO along the [001] axis. Red and yellow circles represent the heptagonal and hexagonal channels, respectively. Pink arrows indicate the placement of Bi at the hexagonal channel.

[1] projection. The HAADF-STEM image of MoVO showed no elements in both the hexagonal and heptagonal channels as we showed previously.[62,63] On the other hand, white spots were clearly observed at the hexagonal channels in MoVBiO (as shown by pink arrows as examples), though only black spots were observed at the heptagonal channels. These findings clearly indicate that metals are placed at the hexagonal channels and no metals are placed at the heptagonal channels. The white spots observed in the hexagonal channels are considered to be Bi since no metals could be seen at the hexagonal channels in MoVO,[62,63] being in agreement with the IR characterization.

XRD simulation was then carried out in order to support the location of Bi at the hexagonal channel since an HAADF-STEM

image can provide structural information only in a limited area. Figure S3 (A) shows experimentally obtained XRD patterns of MoVO and MoVBiO from 12°~18°. Compared with MoVO, the XRD peak intensities at 15.9°, 16.2°, and 17.3°, attributed to (240), (330), and (150) planes, respectively, were clearly decreased by the introduction of Bi. In addition, the peak intensity ratios between (040) and (140) ($Int_{(040)}/Int_{(140)}$) and (320) to (140) ($Int_{(320)}/Int_{(140)}$) were decreased in MoVBiO. Figure S3 (B) shows the results of XRD simulation. Simulation XRD patterns were obtained from the structural model of MoVO containing Bi inside the hexagonal channel with Bi occupancy from 0% to 30%. The basic structural model was obtained by single crystal analysis of MoVO.[54] Although there are differences from the experimentally obtained XRD pattern, possibly due to small changes in the basic crystal structure (occupancy, atomic position, etc.), decreases in the intensities of diffraction peaks at (240), (330), and (150) were observed due to the location of Bi inside the hexagonal channel. In addition, the relative XRD peak intensity ratios, $Int_{(040)}/Int_{(140)}$ and $Int_{(320)}/Int_{(140)}$, were continuously decreased by the increase in Bi occupancy (Figure S3 (C)). When Mo or V was assumed to be placed at the hexagonal channel in the XRD simulation experiment, the decrease of the peak intensity at (320), (330), and (150) was not significant compared with the case of Bi (Figure S3 (D)). Accordingly, the observed changes in XRD peak intensity caused by the introduction of Bi can be explained when Bi is assumed to be located at the hexagonal channel. This is consistent with the results of IR and HAADF-STEM analyses. On the basis of these experimental facts, we concluded that Bi is located at the hexagonal channel. Occupancy of Bi at the hexagonal channel was calculated to be 30% by ICP. It is noted that the Bi occupancy cannot be increased upper than 30% up to this time in spite of the increase of the Bi amount in the preparative conditions, and we are now addressing to increase the Bi occupancy.

Next, the location site of $EtNH_3^+$ was investigated. Figure 6A shows N_2 adsorption isotherms of MoVO-AC, MoVBiO, and MoVBiO-AC (AC: after air calcination at 400 °C for 2 h). After the air calcination, no impurities were formed in MoVO-AC and MoVBiO-AC (Figure S4).[52,54] In the case of MoVBiO-AC, characteristic XRD peak intensity changes caused by the introduction of Bi inside the hexagonal channel were still observed (Figure S4), indicating that Bi is located at the hexagonal channel even after calcination. In the N_2 adsorption experiment, MoVO-AC showed N_2 adsorption at a relative pressure (P/P_0) lower than 1.0×10^{-5}, indicative of microporosity.[15] We have reported that the empty heptagonal channel of MoVO can act as a micropore of 4.0 Å in diameter.[54,64] MoVBiO-AC showed an N_2 adsorption isotherm comparable to that of MoVO-AC. Since no microporosity was observed when atoms were located at the heptagonal channel, Bi should not be located at the heptagonal channel.[25] The results of HAADF-STEM analysis are in agreement with this observation. Micropore volume and external surface area were determined by the t-plot method ($0.15 \le t \le 0.90$) and are shown in Table 1. MoVO-AC and MoVBiO-AC showed almost the same micropore volume (MoVO-AC, 13.0×10^{-3} cm^3 g^{-1}; MoVBiO-AC, 11.6×10^{-3} cm^3 g^{-1}). The external surface area of MoVBiO-AC was 9.5 m^2 g^{-1}, which was 1.6-times larger than that of MoVO-AC (5.8 m^2 g^{-1}) presumably due to the decreased crystal size as observed by SEM. On the other hand, MoVBiO without air calcination showed almost no adsorption at low P/P_0. Figure 6B shows TPD profiles of MoVBiO and MoVBiO-AC. The mass numbers shown in Figure 6B are m/z = 44 (CO_2 or $EtNH_2$) and 45 ($EtNH_2$). More detailed TPD profiles of MoVBiO are shown in Figure S5. Desorption of CO_2 and $EtNH_2$ at 270, 400, 480, and 520 °C (Figure 6B, solid line) were observed in MoVBiO. It has been reported that physically adsorbed species over crystalline Mo_3VO_x materials desorb at a temperature around 150 °C in TPD, which is a much lower temperature than those observed in the TPD measurement.[54,65] Thus, $EtNH_3^+$ should be chemisorbed on or in the structure. After the air calcination, almost no desorption of these species was observed other than the slight desorption of CO_2 or $EtNH_2$ at 480 °C, indicating that almost all of the chemical species were removed by air calcination. This was also confirmed by IR analysis as shown in Figure S6, in which no bands related to the countercation were observed after air calcination. Furthermore, since microporosity was observed after air calcination, we assume that $EtNH_3^+$ is located in the heptagonal channel prior to air calcination. This assumption is reasonable in the sense of the molecular size of $EtNH_3^+$. The size of $EtNH_2$ was calculated using the DMol3 program of Materials Studio 7.1 (Accelrys) to be 0.38 and 0.49 nm in a vertical (minimum) and a horizontal configuration (maximum), respectively. Considering the size of the hexagonal channel (0.25 nm), $EtNH_3^+$ cannot be located in the hexagonal channel (Figure S7). In addition, it might be difficult for $EtNH_3^+$ to be accommodated in the heptagonal channel with a horizontal configuration due to its molecular size. Therefore, we assumed that $EtNH_3^+$ is located at the heptagonal channel in a vertical configuration.

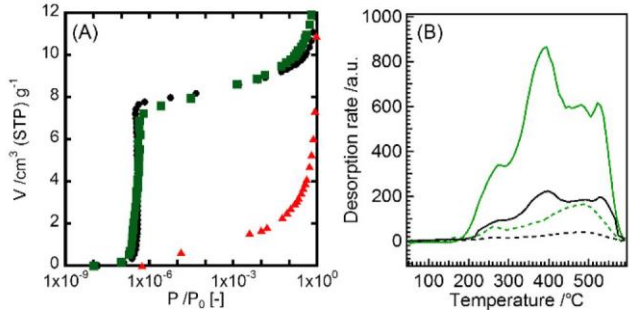

Figure 6. (A) N_2 adsorption isotherms of MoVO-AC (●), MoVBiO (▲), and MoVBiO-AC (■) measured under liquid N_2 temperature. (B) TPD profiles of MoVBiO (solid line) and MoVBiO-AC (dotted line). m/z = 44 (CO_2 or $EtNH_2$), green; m/z = 45 ($EtNH_2$), black.

The amount of $EtNH_3^+$ in the heptagonal channel was estimated by CHN elemental analysis. The obtained C/H/N value of MoVBiO was 1.00/0.62/0.52 wt %. Since MoVO contained no C species (MoVO: C/H/N = 0.00/0.65/0.95 wt %), the observed C value of MoVBiO should be derived from $EtNH_3^+$ as observed by IR and TPD. According to the results of TPD and N_2 adsorption, $EtNH_3^+$ should be occluded in the heptagonal channel. Thus, the chemical composition of MoVBiO can be calculated. If we assume that the C species of MoVBiO is all attributed to $EtNH_3^+$, the weight percent of C, H, and N can be calculated on the basis of the composition of $EtNH_3^+$ to be C/H/N = 1.00/0.38/0.58 wt %. The calculated C/N value was almost the same as the experimentally obtained C/N value, though H was clearly in excess (0.65−0.38 = 0.27 wt %). This excess H might be derived from physically adsorbed H_2O since desorption of H_2O was observed in TPD in the temperature range of 100~200 °C, temperature at which physically adsorbed species desorb

(Figure S5). It was shown that MoVBiO has the same structural framework as that of MoVO and contains Bi in the hexagonal channel. The structural framework composition can thus be calculated to be $Mo_{30.5}V_{9.5}Bi_{1.2}O_{112}$ by using the results of ICP. When the composition of MoVBiO was assumed to be $Mo_{30.5}V_{9.5}Bi_{1.2}O_{112}(EtNH_3)_x{\cdot}yH_2O$, where x and y are the numbers of $EtNH_3^+$ and H_2O, x and y were calculated from the results of C/H/N analysis to be 2.4 and 8.2, respectively. The number of $EtNH_3^+$ in the unit cell (2.4) is clearly smaller than the numbers of heptagonal channels in the unit cell (4), and the occupancy of $EtNH_3^+$ was calculated to be 60%. This agrees with our assumption that $EtNH_3^+$ is located at the heptagonal channel with a vertical configuration because the longer length of $EtNH_3^+$ (0.49 nm) than the c direction of the unit cell (0.40 nm) prevents a periodic array of $EtNH_3^+$ along the layer. However, theoretically, one positive charge is needed per heptagonal channel to compensate the charge balance.[52] Possibly, H^+ is incorporated together with $EtNH_3^+$ into the heptagonal channel, which would compensate the charge balance in the heptagonal channel.

On the basis of these results, the structural model of MoVBiO was obtained. In order to confirm the validity of our proposed structural model, Rietveld refinement was carried out. In accordance with the XPS spectra (Figure S8), the oxidation state of Mo and V in MoVO and MoVBiO was comparable, implying that the charge balance change caused by the introduction of Bi inside the crystal structure is compensated by Bi (3+ as implied by XPS) and coordinating anions. In this time, since we could not represent the coordination of Bi accurately, we added Bi as cations in the Rietveld refinement. Figure 7 shows the results of Rietveld refinement. In this

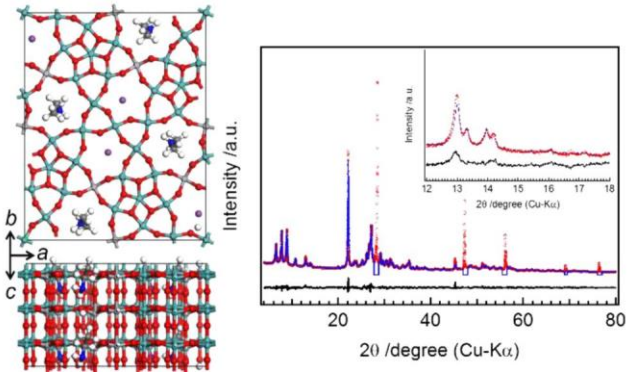

Figure 7. Left: Structural model obtained by Rietveld refinement. Mo, light green; V, gray; O, red; dark gray, C; blue, N; white, H. Right: Difference (black), calculated (blue line), and observed (red •) patterns from Rietveld refinement obtained by using XRD data of MoVBiO at room temperature. XRD peaks of 27.8°~28.8°, 47°~48°, 56°~56.5°, 69°~69.5°, and 76°~77° were attributed to powdered Si added in order to remove orientation effects and were excluded in Rietveld refinement. The inset shows the XRD pattern in the range of 12°~18°.

experiment, the XRD pattern was measured with powdered Si as an external standard to correct the peak positions and to exclude an orientation effect. The XRD peaks of Si were excluded from the refinement. The experimentally obtained pattern (red) and the simulated pattern (blue) matched well, and the R_{wp} value, which represents the difference between these patterns, was 4.9%. This fitting strongly supports the validity of our proposed structure (Figure 7A). On the basis of these results, we concluded that MoVBiO contains $EtNH_3^+$ inside the heptagonal channel with a vertical configuration and 60% occupancy and contains Bi inside the hexagonal channel with 30% occupancy.

So far, orthorhombic MoVBiO containing Bi periodically inside the crystal structure has not been reported. Ammonium ions, typical counter cations in traditional syntheses of Mo−V-based materials, are considerably smaller than the size of the heptagonal channel (NH_4^+, 0.28 nm; heptagonal channel, 0.40 nm). Therefore, it might be difficult for NH_4^+ to accommodate and stabilize the heptagonal channel during the formation of MoVO when Bi is present and lead to the formation of different thermodynamically favored crystal phases (MoO_3 and $(NH_4)_{2.8}H_{0.9}[\varepsilon\text{-}VMo_{9.4}V_{2.6}O_{40}Bi_2]$). Accordingly, we consider that the use of a countercation with a larger size than that of NH_4^+ is crucial for the formation of MoVBiO. In order to assess this hypothesis, MoVBiO was synthesized using different Mo sources, metylammonium heptamolybdate (MAHM, counter-cation: $CH_3NH_3^+$) and dimethylammonium trimolybdate (DMATM, countercation: $(CH_3)_2NH_2^+$).[52] The synthesized materials are abbreviated as MoVBiO (MAHM)-fresh and MoVBiO (DMATM)-fresh, respectively. The size of CH_3NH_2 was calculated to be 0.25 nm in a vertical configuration (minimum) and 0.37 nm in a horizontal configuration (maximum) and the size of $(CH_3)_2NH$ was calculated to be 0.37 nm in a vertical configuration (minimum) and 0.49 nm in a horizontal configuration (maximum) (Figure S7). XRD patterns of the obtained materials are shown in Figure S9. The use of these Mo sources led to the formation of MoVBiO as well as EATM and differed from AHM. These results strongly support our hypothesis that the size of the countercation is critical for the formation of MoVBiO. Thus, we concluded that counter cations of appropriate sizes can work as structure-directing agents for the formation of MoVBiO by accommodat-ing and stabilizing the heptagonal channel during the crystal formation process. This concept may be the fundamental principle for introduction of an additional metal into the MoVO structure.

Selective (amm)oxidation of Light Alkanes. First, selective oxidation of ethane using MoVO and MoVBiO was carried out. For the reaction, MoVO and MoVBiO were heat-treated at 400 °C for 2 h under 50 mL min^{-1} of N_2 flow (MoVO-NT and MoVBiO-NT). After the heat treatment, the countercation species were removed as confirmed by IR spectroscopy (Figure S6).[15] No XRD peaks related to impurities were observed in either of the catalysts before and after the reaction, indicating a high thermal stability of these materials during the reaction (Figures S4 and S10).[15] In addition, characteristic changes in XRD peak intensity caused by the introduction of Bi inside the hexagonal channel were observed after the reaction, indicating that Bi was being located at the hexagonal channel during the reaction. Figure 8 shows ethane conversion and product selectivity over MoVO-NT and MoVBiO-NT as a function of reaction temperature. For MoVO-NT, the ethane conversion increased with an increase in reaction temperature and the conversion at 300 °C was 27.3%. The observed products were ethylene, CO_x, and acetic acid. The selectivity of ethylene was over 90% when the reaction temperature was below 300 °C. At temperature above 300 °C, the selectivity of CO_x increased gradually with a decrease in ethylene selectivity. The selectivity of acetic acid was always less than 3% regardless of the reaction temperature. In the case of MoVBiO-NT, almost the same ethane conversion

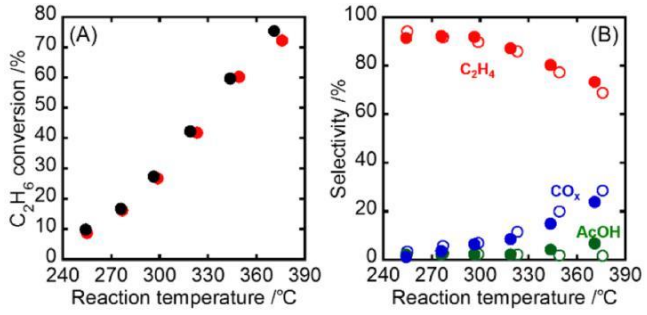

Figure 8. (A) Conversion and (B) selectivity changes as a function of reaction temperature in oxidative dehydrogenation of ethane over MoVO-NT and MoVBiO-NT. (A) Rates of ethane conversion over MoVO-NT (black •) and MoVBiO-NT (red •) are plotted. (B) Product selectivities over MoVO-NT (closed symbols) and MoVBiO-NT (open symbols) are plotted. Reaction conditions: catalyst amount, 0.5 g; gas feed, $C_2H_6/O_2/N_2$ = 5/5/40 mL min^{-1}.

and product selectivity as those with MoVO-NT were observed at all reaction temperatures. We have reported that ethane was converted to ethylene inside an empty heptagonal channel of the structure and that almost no conversion occurred over the catalyst surface in our examined temperature range.[21−23,53] MoVBiO has empty heptagonal channels as confirmed by N_2 adsorption, and almost the same catalytic activity was therefore observed regardless of the introduction of Bi inside the structure.

For the ammoxidation of propane, MoVO-NT and MoVBiO-NT were used as catalysts as well as for ethane oxidation. The catalysts were heat-treated at 420 °C for 0.5 h under reaction conditions prior to the reaction. After the catalytic reaction, no XRD peaks related to impurities were observed (Figure S10). In this case, characteristic changes in XRD peak intensity caused by the introduction of Bi inside the hexagonal channel were observed after the reaction, indicating placement of Bi in the hexagonal channel during the reaction. Figure 9 shows propane conversion and product selectivity as a function of reaction temperature over MoVO-NT and MoVBiO-NT. Figure 9A shows the catalytic activities of MoVO-NT and MoVBiO-NT with the same catalyst amounts (0.2 g). Both the propane conversion and oxygen conversion of MoVBiO-NT were much higher than those of MoVO-NT at all reaction temperatures. Higher CO_2 selectivity was observed in MoVBiO-NT than in MoVO-NT at all reaction temperatures due to the high rates of propane and oxygen conversion. Therefore, product selectivities were compared at the same rate of conversion by changing the amount of the catalyst (Figure 9C and D). For this purpose, 0.3 g of MoVO-NT and 0.1 g of MoVBiO-NT were used. As can be seen in Figure 9C, the rate of propane and oxygen conversion over these catalysts were almost the same at all reaction temperatures. Since 0.1 g of MoVBiO-NT showed the same catalytic activity as that of 0.3 g of MoVO-NT, the catalytic activity of MoVBiO-NT is almost 3-times higher than that of MoVO-NT. Table 2 shows the results for N_2 and propane adsorption over MoVO-NT and MoVBiO-NT after propane ammoxidation (MoVO-amm and MoVBiO-amm, respectively). The adsorption isotherms are shown in Figures S11 and S12, respectively. After the reaction, the external surface areas of MoVO-amm and MoVBiO-amm were slightly increased to 6.7 and 10.7 m^2 g^{-1}, respectively. There was only a 1.6-times difference between their external surface areas, and the catalytic activity per unit cell of MoVBiO-

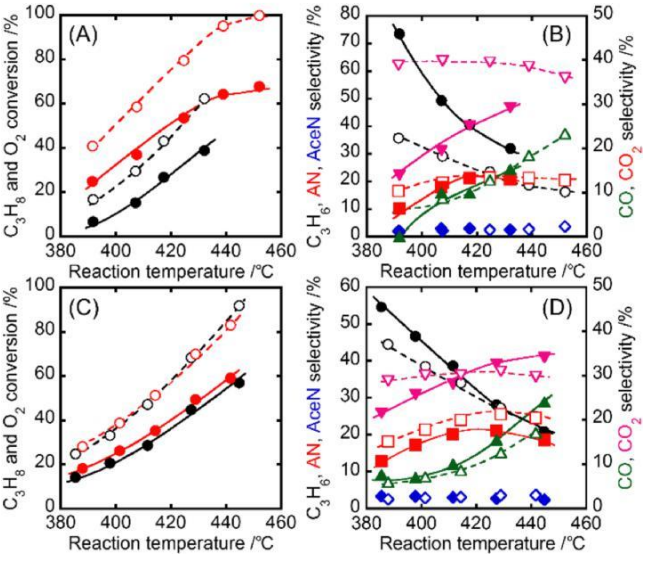

Figure 9. (A) and (C) Conversion and (B) selectivity, (D) changes as a function of reaction temperature in propane ammoxidation over MoVO-NT and MoVBiO-NT. (A and C) Rates of propane conversion (solid symbols) and oxygen conversion (open symbols) are plotted. MoVO-NT, black; MoVBiO-NT, red. (B and D) Product selectivities of propylene (C_3H_6, circle), acrylonitrile (AN, square), acetonitrile (AceN, lozenge), CO (triangle), and CO_2 (inversed triangle). MoVO-NT, closed symbols; MoVBiO-NT, open symbols. (A and B) Reaction conditions: catalyst amount, 0.2 g; gas feed, $C_3H_8/O_2/NH_3/He$ = 3.0/ 9.0/4.0/34.0 mL min^{-1}. (C and D) Reaction conditions: catalyst amount, 0.3 g (MoVO-NT) and 0.1 g (MoVBiO-NT); gas feed, $C_3H_8/O_2/NH_3/He$ = 3.0/9.0/4.0/34.0 mL min^{-1}.

Table 2. Results of N_2 and Propane Adsorption of MoVO and MoVBiO after Propane Ammoxidation

		micropore volume (10^{-3} cm^3 g^{-1})	
catalyst	external surface area[a] (m^2 g^{-1})	N_2[a]	propane[b]
MoVO-amm	6.7	5.0	8.1
MoVBiO-amm	10.7	11.0	14.3

[a]Measured by N_2 adsorption at liq. N_2 temperature and estimated by the t-plot method. [b]Measured by propane adsorption at 25 °C and estimated by the DA method.

NT is thus 1.9-times higher than that of MoVO-NT. In order to understand the increased catalytic activity of MoVBiO-NT, the microporosity of MoVO-amm and MoVBiO-amm derived from the heptagonal channel was evaluated since it has been reported that the heptagonal channel is strongly related to the activation of propane.[22] The micropore volume of MoVO-amm estimated by N_2 adsorption was 5.0 × 10^{-3} cm^3 g^{-1}, which was clearly lower than that observed prior to the reaction. The decreased micropore volume of MoVO-amm compared with that prior to the reaction is due to the reduction state change during the reaction, as the reduction state of MoVO strongly affects the micropore size, resulting in the prevention of access of N_2 to the micropore.[54,65] On the other hand, MoVBiO-amm showed micropore adsorption even after the reaction, and the estimated micropore volume was 11.0 × 10^{-3} cm^3 g^{-1}. UV spectra indicated that the reduction states of MoVO-amm and MoVBiO-amm were comparable (Figure-S13). These results imply that the intrinsic heptagonal channel size of MoVBiO is sufficient to accept N_2 even after the decrease in micropore size due to the change in the reduction state. Propane adsorption

was also carried out in order to evaluate the accessibility of propane into the heptagonal channel.[54] Figure S12 shows propane adsorption isotherms of MoVO-amm and MoVBiO-amm. The amount of propane adsorption of MoVBiO-amm was clearly larger than that of MoVO-amm, and the micropore volumes estimated by the DA method were 8.1×10^{-3} and 14.3×10^{-3} cm^3 g^{-1} for MoVO-amm and MoVBiO-amm, respectively (Table 2), indicating that the filling rates of propane inside the heptagonal channel were 36% and 64%, respectively. The difference in micropore volumes estimated by N_2 or propane adsorption is due to the difference in adsorption temperature (N_2 adsorption, −196 °C; propane adsorption, 25 °C), which affects the diffusion of molecules.[54,66] The molecular size of propane has been reported to be 0.43 nm, which is slightly larger than that of the heptagonal channel (0.40 nm).[54] The increase in propane adsorption capacity in MoVBiO-amm also supports the assumption that the heptagonal channel size was expanded by the introduction of Bi. Therefore, we suggest that the introduction of Bi into the hexagonal channel expanded the size of the heptagonal channel by partial modification of the lattice size (note: lattice parameters were increased as indicated by XRD), which led to strong interaction between the heptagonal channel and propane, resulting in an increase of the propane conversion. As shown in Figure 9D, the propylene selectivity over MoVO-NT was ca. 54.6% at 385.4 °C and the value was decreased with an increase in reaction temperature, reaching 20.9% at 444.7 °C. With a decrease in propylene selectivity, the selectivities to acrylonitrile (AN), CO, and CO_2 increased. The AN selectivity at 385.4 °C was 12.9% and increased with an increase in reaction temperature, reaching 21.1% at 427.3 °C. Further increase in the reaction temperature decreased the AN selectivity, and it was 18.6% at 444.7 °C. Acetonitrile (AceN) selectivity was almost unchanged with increase in reaction temperature, and it was ca. 2−3%. For MoVBiO-NT, the selectivity of propylene at 387.9 °C was 44.5% and it was lower than that for MoVO-NT at a similar reaction temperature. With increase in the reaction temperature, propylene selectivity decreased. However, the decrease in selectivity was moderate compared with that MoVO-NT, and propylene selectivity at 441.6 °C was 24.9%. AN selectivity over MoVBiO-NT was slightly higher than that over MoVO-NT at all reaction temperatures, and AN selectivities were 18.2% at 387.9 °C and 25.5% at 428.9 °C. A striking effect of Bi on AN selectivity was observed at high temperatures. Although a decrease in AN selectivity was observed at high temperatures in MoVO-NT (427.3 °C, 21.1%; 444.7 °C, 18.6%), AN selectivity of MoVBiO-NT was maintained almost at the same level even at high temperatures (428.9 °C, 25.5%; 441.6 °C, 24.6%). The effect of a Bi promoter on an MoVTeNbO catalyst was recently studied by Andrushkevich et al., and they reported that the addition of Bi resulted in the maintenance of acrylonitrile selectivity in a range in which the propane conversion was high (over 80%).[50] They suggested that the addition of Bi decreased the acidity of the catalyst due to the high basicity of Bi, which facilitated easy desorption of AN from the catalyst surface since AN has a basic nature. Therefore, the decomposition of AN was suppressed by the addition of Bi, resulting in high AN selectivity. On the basis of this perspective, we evaluated the acid−base characters of MoVO-amm and MoVBiO-amm by ammonia TPD. Figure S14 shows the results of ammonia TPD for MoVO-amm and MoVBiO-amm. The acid concentration of MoVBiO-amm was lower than that of MoVO-amm (MoVBiO-amm, 0.131 mmol g^{-1}; MoVO-amm, 0.207 mmol g^{-1}). We now consider that the introduction of Bi increased the surface basicity over the catalyst, which suppressed the decomposition of AN, resulting in high AN selectivity, especially at high rates of propane conversion.

When AN selectivity is compared with other crystalline Mo−V−M−O catalysts (M = Te or Sb), AN selectivity over MoVBiO was apparently low (AN selectivity: MoVTeO, 38.8% at 47.7% C_3H_8 conversion (410 °C); MoVSbO, 48.9% at 42.5% C_3H_8 conversion (410 °C)), although the experimental conditions were different.[36] In our case, the Bi occupancy in the hexagonal channel was not so high (30%) which might enshroud the catalytic function of Bi. We are now trying to increase the Bi occupancy in MoVBiO for the deep understanding of the catalytic role of Bi for propane ammoxidation.

We conclude that although almost no difference was observed in the catalytic activities of MoVO-NT and MoVBiO-NT for selective oxidation of ethane, propane conversion in the ammoxidation of propane was significantly enhanced by the introduction of Bi, possibly due to the expanded micropore size, and the introduction of Bi affected the acid−base property of the catalyst, resulting in an increase in AN selectivity.

CONCLUSIONS

We successfully synthesized orthorhombic Mo−V−Bi oxide (MoVBiO) having the same crystal structure as that of orthorhombic Mo_3VO_x (MoVO) for the first time by using ethylammonium cation ($EtNH_3^+$) as a structure-directing agent. Structural analysis clearly demonstrated that Bi is located at the hexagonal channel and that $EtNH_3^+$ is located at the heptagonal channel. The catalytic activity of MoVBiO for selective oxidation of ethane was comparable to that of MoVO. However, for ammoxidation of propane, the rate of propane conversion over MoVBiO was much higher than that over MoVO. Expansion of the heptagonal channel by the introduction of Bi enhanced the interaction between propane and the heptagonal channel, which might have resulted in the increase in propane conversion. A comparison of product selectivities at comparable conversion rates revealed that the introduction of Bi enhanced acrylonitrile selectivity, especially at high temperatures (ca. 440 °C). The introduction of Bi potentially increases the surface basicity over the catalyst, which can accelerate the desorption of acrylonitrile, resulting in enhanced selectivity. The results demonstrate a successful strategy to design crystalline Mo−V-based mixed oxide catalysts by the use of structure-directing agents. Furthermore, this strategy will enable multifunctionalization of a catalyst by the introduction of additional metals inside the crystal structure, periodically, at a nanoscale.

ASSOCIATED CONTENT

* Supporting Information

XPS data for MoVBiO; XRD pattern of MoVBiO (AHM)-fresh; simulation XRD patterns of MoVBiO; XRD patterns of MoVBiO after heat treatments; TPD spectrum of MoVBiO; IR spectra of MoVBiO after heat treatments; molecular sizes of amines; XPS spectra of Mo

and V for MoVO and MoVBiO; XRD patterns of MoVBiO synthesized with various Mo sources, XRD patterns of MoVO and MoVBiO after catalytic reactions; N_2 adsorption isotherms of MoVO and MoVBiO after ammoxidation of propane; propane adsorption isotherms after ammoxidation of propane; UV spectra of MoVO and MoVBiO after ammoxidation of propane; results of ammonia TPD of MoVO and MoVBiO after ammox-idation of propane (PDF)

AUTHOR INFORMATION

Corresponding Author

*E-mail: uedaw@kanagawa-u.ac.jp.

ORCID

Satoshi Ishikawa: 0000-0003-4372-4108

Masahiro Sadakane: 0000-0001-7308-563X

Author Contributions

The manuscript was written through contributions of all authors. All authors have given approval to the final version of the manuscript.

Notes

The authors declare no competing financial interest.

ACKNOWLEDGMENTS

This work was supported by JSPS KAKENHI Grant 2324-6135.

REFERENCES

(1) Grasselli, R. K. Site Isolation and Phase Cooperation: Two Important Concepts in Selective Oxidation Catalysis: A Retrospective. Catal. Today 2014, 238, 10−27.

(2) Mizuno, N.; Misono, M. Heterogeneous Catalysis. Chem. Rev. 1998, 98, 199−217.

(3) Koyano, G.; Saito, T.; Misono, M. In Situ Vibrational Spectroscopic Investigation of Surface Redox Process of Vanadyl Pyrophosphate. J. Mol. Catal. A: Chem. 2000, 155, 31−41.

(4) Thomas, J. M.; Raja, R.; Sankar, G.; Bell, R. G. Molecular-Sieve Catalysts for the Selective Oxidation of Linear Alkanes by Molecular Oxygen. Nature 1999, 398, 227−230.

(5) Thomas, J. M.; Raja, R. Design of a "Green" One-Step Catalytic Production of ε-caprolactam (Precursor of Nylon-6). Proc. Natl. Acad. Sci. U. S. A. 2005, 102, 13732−13736.

(6) Batiot, C.; Hodnett, B. K. The Role of Reactant and Product Bond Energies in Determining Limitations to Selective Catalytic Oxidations. Appl. Catal., A 1996, 137, 179−191.

(7) Sun, M.; Zhang, J.; Putaj, P.; Caps, V.; Lefebvre, F.; Pelletier, J.; Basset, J. M. Catalytic Oxidation of Light Alkanes (C1−C4) by Heteropoly Compounds. Chem. Rev. 2014, 114, 981−1019.

(8) Grasselli, R. K. Fundamental Principle of Selective Heterogeneous Oxidation Catalysis. Top. Catal. 2002, 21, 79−88.

(9) Thomas, J. M.; Raja, R.; Sankar, G.; Bell, R. G. Molecular Sieve Catalysts for the Regioselective and Shape-Selective Oxyfunctionalization of Alkanes in Air. Acc. Chem. Res. 2001, 34, 191−200.

(10) Moro-oka, Y.; Ueda, W.; Lee, K. H. The Role of Bulk Oxide Ion in the Catalytic Oxidation Reaction over Metal Oxide Catalyst. J. Mol. Catal. A: Chem. 2003, 199, 139−148.

(11) Vedrine, J. C. Revisiting Active Sites in Heterogeneous Catalysis: Their Structure and Their Dynamic Behavior. Appl. Catal., A 2014, 474, 40−50.

(12) Katou, T.; Vitry, D.; Ueda, W. Hydrothermal Synthesis of a New Mo-V-O Complex Metal Oxide and Its Catalytic Activity for the Oxidation of Propane. Chem. Lett. 2003, 32, 1028−1029.

(13) Ueda, W.; Vitry, D.; Katou, T. Structural Organization of Catalytic Functions in Mo-based Oxides for Propane Selective Oxidation. Catal. Today 2004, 96, 235−240.

(14) Ueda, W.; Vitry, D.; Katou, T. Crystalline Mo-V-O Based Complex Oxides as Selective Oxidation Catalysts of Propane. Catal. Today 2005, 99, 43−49.

(15) Konya, T.; Katou, T.; Murayama, T.; Ishikawa, S.; Sadakane, M.; Buttrey, D. J.; Ueda, W. An Orthorhombic Mo_3VO_x Catalyst Most Active for Oxidative Dehydrogenation of Ethane among Related Complex Metal Oxides. Catal. Sci. Technol. 2013, 3, 380−387.

(16) Wang, F.; Ueda, W. Aerobic Oxidation of Alcohols over Novel Crystalline MoVO Oxide. Appl. Catal., A 2008, 346, 155−163.

(17) Wang, F.; Ueda, W. Selective Oxidation of Alcohols using Novel Crystalline Mo-V-O Oxide as Heterogeneous Catalyst in Liquid Phase with Molecular Oxygen. Catal. Today 2009, 144, 358−361.

(18) Murayama, T.; Katryniok, B.; Heyte, S.; Araque, M.; Ishikawa, S.; Dumeignil, F.; Paul, S.; Ueda, W. Role of Crystalline Structure in Allyl Alcohol Selective Oxidation over Mo_3VO_x Complex Metal Oxide Catalysts. ChemCatChem 2016, 8, 2415−2420.

(19) Chen, C.; Kosuke, N.; Murayama, T.; Ueda, W. Single-Crystalline-Phase Mo_3VO_x: An Efficient Catalyst for the Partial Oxidation of Acrolein to Acrylic Acid. ChemCatChem 2013, 5, 2869− 2873.

(20) Qiu, C.; Chen, C.; Ishikawa, S.; Murayama, T.; Ueda, W. Crystalline Mo-V-W-Mixed Oxide with Orthorhombic and Trigonal Structures as Highly Efficient Oxidation Catalysts of Acrolein to Acrylic Acid. Top. Catal. 2014, 57, 1163−1170.

(21) Ishikawa, S.; Yi, X.; Murayama, T.; Ueda, W. Heptagonal Channel Micropore of Orthorhombic Mo_3VO_x as Catalysis Field for the Selective Oxidation of Ethane. Appl. Catal., A 2014, 474, 10−17.

(22) Ishikawa, S.; Yi, X.; Murayama, T.; Ueda, W. Catalysis Field in Orthorhombic Mo_3VO_x Oxide Catalyst for the Selective Oxidation of Ethane, Propane and Acrolein. Catal. Today 2014, 238, 35−40.

(23) Ishikawa, S.; Ueda, W. Microporous Crystalline Mo-V Mixed Oxides for Selective Oxidations. Catal. Sci. Technol. 2016, 6, 617−629.

(24) Hibst, H.; Rosowski, F.; Cox, G. New Cs-Containing Mo-V^{4+} Based Oxides with the Structure of the M1 Phase-Base for New Catalysts for the Direct Alkane Activation. Catal. Today 2006, 117, 234−241.

(25) Sadakane, M.; Yamagata, K.; Kodato, K.; Endo, K.; Toriumi, K.; Ozawa, Y.; Ozeki, T.; Nagai, T.; Matsui, Y.; Sakaguchi, N.; Pyrz, W. D.; Buttrey, D. J.; Blom, D. A.; Vogt, T.; Ueda, W. Synthesis of Orthorhombic Mo-V-Sb Oxide Species by Assembly of Pentagonal Mo_6O_{21} Polyoxometalate Building Blocks. Angew. Chem., Int. Ed. 2009, 48, 3782−3786.

(26) Canioni, R.; Marchal-Roch, C.; Leclerc-Laronze, N.; Haouas, M.; Taulelle, F.; Marrot, J.; Paul, S.; Lamonier, C.; Paul, J. F.; Loridant, S.; Millet, J. M. M.; Cadot, E. Selective Conversion of $\{Mo_{132}\}$ Keplerate Ion into 4-Electron Reduced Crown-Capped Keggin Derivative $[Te_5Mo_{15}O_{57}]^{8-}$. A Key Intermediate to Single-Phase M1Multielement MoVTeO Light-Alkanes Oxidation Catalyst. Chem. Commun. 2011, 47, 6413−6415.

(27) Ushikubo, T.; Oshima, K.; Kayou, A.; Vaarkamp, M.; Hatano, M. Ammoxidation of Propane over Catalysts Comprising Mixed Oxides of Mo and V. J. Catal. 1997, 169, 394−396.

(28) He, Q.; Woo, J.; Belianinov, A.; Guliants, V. V.; Borisevich, A. Y. Better Catalysts through Microscopy: Mesoscale M1/M2 Intergrowth in Molybdenum-Vanadium Based Complex Oxide Catalysts for Propane Ammoxidation. ACS Nano 2015, 9, 3470−3478.

(29) Murayama, H.; Vitry, D.; Ueda, W.; Fuchs, G.; Anne, M.; Dubois, J. L. Structure Characterization of Orthorhombic Phase in MoVTeNbO Catalyst by Powder X-ray Diffraction and XANES. Appl. Catal., A 2007, 318, 137−142.

(30) DeSanto, P., Jr.; Buttrey, D. J.; Grasselli, R. K.; Lugmair, C. G.; Volpe, A. F.; Toby, B. H.; Vogt, T. Structural Characterization of the Orthorhombic Phase M1 in MoVNbTeO Propane Ammoxidation Catalyst. Top. Catal. 2003, 23, 23−38.

(31) Millet, J. M. M.; Roussel, H.; Pigamo, A.; Dubois, J. L.; Jumas, J. C. Characterization of Tellurium in MoVTeNbO Catalysts for Propane Oxidation or Ammoxidation. Appl. Catal., A 2002, 232, 77−92.

(32) Pyrz, W. D.; Blom, D. A.; Vogt, T.; Buttrey, D. J. Direct Imaging of the MoVTeNbO M1 Phase Using An Aberration-Corrected High-Resolution Scanning Transmission Electron Microscope. Angew. Chem., Int. Ed. 2008, 47, 2788−2791.
(33) Grasselli, R. K.; Burrington, J. D.; Buttrey, D. J.; DeSanto, P., Jr.; Lugmair, C. G.; Volpe, A. F., Jr.; Weingand, T. Multifunctionality of Active Centers in (Amm)oxidation Catalysts: From Bi-Mo-O_X to Mo-V-Nb-(Te, Sb)-O_X. Top. Catal. 2003, 23, 5−22.
(34) Grasselli, R. K.; Buttrey, D. J.; Burrington, J. D.; Andersson, A.; Holmberg, J.; Ueda, W.; Kubo, J.; Lugmair, C. G.; Volpe, A. F. Active Centers, Catalytic Behavior, Symbiosis and Redox Properties of MoV(Nb, Ta)TeO Ammoxidation Catalysts. Top. Catal. 2006, 38, 7− 16.
(35) Chieregato, A.; Lopeź Nieto, J. M.; Cavani, F. Mixed-Oxide Catalysts with Vanadium as the Key Element for Gas-Phase Reactions. Coord. Chem. Rev. 2015, 301−302, 3−23.
(36) Watanabe, N.; Ueda, W. Comparative Study on the Catalytic Performance of Single-Phase Mo-V-O-Based Metal Oxide Catalysts in Propane Ammoxidation to Acrylonitrile. Ind. Eng. Chem. Res. 2006, 45, 607−614.
(37) Grasselli, R. K.; Tenhover, M. A. Ammoxidation. In Handbook of Heterogeneous Catalysis, 2nd ed.; Ertl, G., Knozinger, H., Schuïth, G., Weitkamp, J., Eds.; Wiley-VCH: Weinheim, 2008; Vol. 8, pp 3489− 3517.
(38) Guliants, V. V.; Bhandari, R.; Swaminathan, B.; Vasudevan, V. K.; Brongersma, H. H.; Knoester, A.; Gaffney, A. M.; Han, S. Roles of Surface Te, Nb, and Sb Oxides in Propane Oxidation to Acrylic Acid over Bulk Orthorhombic Mo-V-O Phase. J. Phys. Chem. B 2005, 109, 24046−24055.
(39) Guliants, V. V.; Bhandari, R.; Hughett, A. R.; Bhatt, S.; Schuler, B. D.; Brongersma, H. H.; Knoester, A.; Gaffney, A. M.; Han, S. Probe Molecule Chemisorption-Low Energy Ion Scattering Study of Surface Active Sites Present in the Orthorhombic Mo-V-(Te-Nb)-O Catalysts for Propane (Amm)oxidation. J. Phys. Chem. B 2006, 110, 6129−6140.
(40) Grasselli, R. K.; Volpe, A. F. Catalytic Consequences of a Revised Distribution of Key Elements at the Active Centers of the M1 Phase of the $MoVNbTeO_X$ System. Top. Catal. 2014, 57, 1124−1137.
(41) Govindasamy, A.; Muthukumar, K.; Yu, J.; Xu, Y.; Guliants, V. V. Adsorption of Propane, Isopropyl, and Hydrogen on Cluster Models of the M1 Phase of Mo-V-Te-Nb-O Mixed Metal Oxide Catalyst. J. Phys. Chem. C 2010, 114, 4544−4549.
(42) Glaeser, L. C.; Brazdil, J. F.; Hazle, M. A.; Mehicic, M.; Grasselli, R. K. Identification of Active Oxide Ions in a Bismuth Molybdate Selective Oxidation Catalyst. J. Chem. Soc., Faraday Trans. 1 1985, 81, 2903−2912.
(43) Brazdil, J. F. Scheelite: a Versatile Structural Template for Selective Alkene Oxidation Catalysts. Catal. Sci. Technol. 2015, 5, 3452−3458.
(44) Zhai, Z.; Getsoian, A. B.; Bell, A. T. The Kinetics of Selective Oxidation of Propene on Bismuth Vanadium Molybdenum Oxide Catalysts. J. Catal. 2013, 308, 25−36.
(45) Ueda, W.; Moro-oka, Y.; Ikawa, T. ^{18}O Tracer Study of the Active Species of Oxygen on Bi_2MoO_6 Catalyst. J. Chem. Soc., Faraday Trans. 1 1982, 78, 495−500.
(46) Jang, Y. H.; Goddard, W. A., III Selective Oxidation and Ammoxidation of Propene on Bismuth Molybdates, ab initio Calculations. Top. Catal. 2001, 15, 273−289.
(47) Jang, Y. H.; Goddard, W. A. Mechanism of Selective Oxidation and Ammoxidation of Propene on Bismuth Molybdates from DFT Calculations on Model Clusters. J. Phys. Chem. B 2002, 106, 5997− 6013.
(48) Pudar, S.; Oxgaard, J.; Chenoweth, K.; van Duin, A. C. T.; Goddard, W. A. Mechanism of Selective Oxidation of Propene to Acrolein on Bismuth Molybdates from Quantum Mechanical Calculations. J. Phys. Chem. C 2007, 111, 16405−16415.
(49) Deniau, B.; Nguyen, T. T.; Delichere, P.; Safonova, O.; Millet, J. M. M. Redox State Dynamics at the Surface of MoVTe(Sb)NbO M1 Phase in Selective Oxidation of Light Alkanes. Top. Catal. 2013, 56, 1952−1962.
(50) Andrushkevich, T. V.; Popova, G. Y.; Chesalov, Y. A.; Ischenko, E. V.; Khramov, M. I.; Kaichev, V. V. Propane Ammoxidation on Bi Promoted $MoVTeNbO_X$ Oxide Catalysts: Effect of Reaction Mixture Composition. Appl. Catal., A 2015, 506, 109−117.
(51) Ueda, W.; Oshihara, K. Selective Oxidation of Light Alkanes over Hydrothermally Synthesized Mo-V-M-O (M = Al, Ga, Bi, Sb, and Te) Oxide Catalysts. Appl. Catal., A 2000, 200, 135−143.
(52) Ishikawa, S.; Murayama, T.; Ohmura, S.; Sadakane, M.; Ueda, W. Synthesis of Novel Orthorhombic Mo and V Based Complex Oxides Coordinating Alkylammonium Cation in Its Heptagonal Channel and Their Application as a Catalyst. Chem. Mater. 2013, 25, 2211−2219.
(53) Ishikawa, S.; Murayama, T.; Kumaki, M.; Tashiro, M.; Zhang, Z.; Yoshida, A.; Ueda, W. Synthesis of Trigonal Mo-V-M^{3rd}-O (M^{3rd} = Fe, W) Catalysts by Using Structure-Directing Agent and Catalytic Performances for Selective Oxidation of Ethane. Top. Catal. 2016, 59, 1477−1488.
(54) Ishikawa, S.; Kobayashi, D.; Konya, T.; Ohmura, S.; Murayama, T.; Yasuda, N.; Sadakane, M.; Ueda, W. Redox Treatment of Orthorhombic $Mo_{29}V_{11}O_{112}$ and Relationships between Crystal Structure, Microporosity and Catalytic Performance for Selective Oxidation of Ethane. J. Phys. Chem. C 2015, 119, 7195−7206.
(55) Zhang, Z.; Sadakane, M.; Murayama, T.; Izumi, S.; Yasuda, N.; Sakaguchi, N.; Ueda, W. Tetrahedral Connection of ε-Keggin-type Polyoxometalates to Form an All-Inorganic Octahedral Molecular Sieve with an Intrinsic 3D Pore System. Inorg. Chem. 2014, 53, 903− 911.
(56) Zhang, Z.; Sadakane, M.; Murayama, T.; Sakaguchi, N.; Ueda, W. Preparation, Structural Characterization, and Ion-Exchange Properties of Two New Zeolite-like 3D Frameworks Constructed by ε-Keggin-Type Polyoxometalates with Binding Metal Ions, $H_{11.4}[ZnMo_{12}O_{40}Zn_2]^{1.5-}$ and $H_{7.5}[Mn_{0.2}Mo_{12}O_{40}Mn_2]^{2.1-}$. Inorg. Chem. 2014, 53, 7309−7318.
(57) Zhang, Z.; Sadakane, M.; Murayama, T.; Ueda, W. Investigation of the Formation Process of Zeolite-Like 3D Frameworks Constructed with ε-Keggin-Type Polyoxovanadomolybdates with Binding Bismuth Ions and Preparation of a Nano-Crystal. Dalton Trans. 2014, 43, 13584−13590.
(58) Nguyen, T. T.; Deniau, B.; Baca, M.; Millet, J. M. M. Synthesis and Monitoring of MoVSbNbO Oxidation Catalysts Using V K and Sb L_1-Edge XANES Spectroscopy. Top. Catal. 2011, 54, 650−658.
(59) Fripiat, J. J.; Pennequin, M.; Poncelet, G.; Cloos, P. Influence of the Van Der Waals Force on the Infrared Spectra of Short Aliphatic Alkylammonium Cations Held on Montmorillonite. Clay Miner. 1969, 8, 119−134.
(60) Zeegers-Huyskens, T.; Bator, G. Fourier Transform Infrared and Fourier Transform Raman Investigation of Alkylammonium Hexa-chloroantimonates. Vib. Spectrosc. 1996, 13, 41−49.
(61) Oxton, I. A. Vibrational Spectra of Provskite-type Lyer Compounds. Bis(etylammonium)tetrachlorocadmate and propylene-diammonium tetrachlorocadmate. J. Mol. Struct. 1979, 54, 11−18.
(62) Pyrz, W. D.; Blom, D. A.; Sadakane, M.; Kodato, K.; Ueda, W.; Vogt, T.; Buttrey, D. J. Atomic-Scale Investigation of Two-Component MoVO Complex Oxide Catalysts Using Aberration-Corrected High-Angle Annular Dark-Field Imaging. Chem. Mater. 2010, 22, 2033− 2040.
(63) Pyrz, W. D.; Blom, D. A.; Sadakane, M.; Kodato, K.; Ueda, W.; Vogt, T.; Buttrey, D. J. Atomic-Level Imaging of Mo-V-O Complex Oxide Phase Intergrowth, Grain Boundaries, and Defects using HAADF-STEM. Proc. Natl. Acad. Sci. U. S. A. 2010, 107, 6152−6157.
(64) Sadakane, M.; Kodato, K.; Kuranishi, T.; Nodasaka, Y.; Sugawara, K.; Sakaguchi, N.; Nagai, T.; Matsui, Y.; Ueda, W. Molybdenum-Vanadium-Based Molecular Sieves with Microchannels of Seven-Membered Rings of Corner-Sharing Metal Oxide Octahedra. Angew. Chem., Int. Ed. 2008, 47, 2493−2496.
(65) Sadakane, M.; Ohmura, S.; Kodato, K.; Fujisawa, T.; Kato, K.; Shimidzu, K.; Murayama, T.; Ueda, W. Redox Tunable Reversible Molecular Sieves: Orthorhombic Molybdenum Vanadium Oxide. Chem. Commun. 2011, 47, 10812−10814.

.

(66) Luo, J.; Zhang, Q.; Garcia-Martinez, J.; Suib, S. L. Adsorptive and Acidic Properties, Reversible Lattice Oxygen Evolution, and Catalytic Mechanism of Cryptomelane-Type Manganese Oxides as Oxidation Catalysts. J. Am. Chem. Soc. 2008, 130, 3198−3207.